ELSEVIER

Journal of Fluids and Structures 24 (2008) 994–1005

JOURNAL OF FLUIDS AND STRUCTURES

www.elsevier.com/locate/jfs

Transition phenomena in the wake of an inclined square cylinder

X.H. Tong[1], S.C. Luo*, B.C. Khoo

Department of Mechanical Engineering, National University of Singapore, 10 Kent Ridge Crescent, Singapore 119260, Singapore

Received 11 June 2007; accepted 2 March 2008
Available online 7 May 2008

Abstract

The division of flow regimes in a square cylinder wake at various angles of attack (α) is studied. This study provides evidence of the existence of modes A and B instabilities in the wake of an inclined square cylinder. The critical Reynolds numbers for the inception of these instability modes were identified through the determination of discontinuities in the Strouhal number versus Reynolds number curves. The spectra and time traces of wake streamwise velocity were observed to display three distinct patterns in different flow regimes. Streamwise vortices with different wavelengths at various Reynolds numbers were visualized. A PIV technique was employed to quantitatively measure the parameters of wake vortices. The wavelengths of the streamwise vortices in the modes A and B regimes were measured by using the auto-correlation method. From the present investigation, the square cylinder wake at various angles of attack undergoes a similar transition path to that of a circular cylinder, although various quantitative parameters measured which include the critical Reynolds numbers, spanwise wavelength of secondary vortices, and the circulation and vorticity of wake vortices all show an α dependence.

1. Introduction

In the authors' earlier paper (Luo et al., 2007), the transition phenomena in the wake of a normal square cylinder (at no angle of attack, with one side normal to the oncoming free stream) had been investigated and reported in detail. In the Introduction in Luo et al. (2007), a detailed review of the transitional phenomena in the wake of a circular cylinder was first given. Very briefly, it was established that the circular cylinder wake transition involves two modes (modes A and B) of small-scale 3-D instability, which are related to the two discontinuities in the St–Re (Strouhal number versus Reynolds number) relation. For circular cylinder wakes, mode A is evident in the range $190 < Re < 240$, while mode B can be observed starting from Re of about 240. A review of some important findings can be found in Williamson (1996a). For square cylinder wakes, Luo et al. (2007) showed that essentially the two modes of 3-D instability also exist, but with lower critical Reynolds numbers of approximately 160 and 204 for transition to modes A and B instability, respectively. The spanwise wavelengths of the two modes of instability are also larger than their circular cylinder counterparts. A lack in experimental work on square cylinder wake transition phenomena was also noted. Interested readers are referred to Luo et al. (2007) for more details.

*Corresponding author.
E-mail address: mpeluosc@nus.edu.sg (S.C. Luo).
[1]Present address: China Knowledge Consulting, 8 Temasek Boulevard, #37-01A Suntec Tower Three, Singapore 038988, Singapore.

0889-9746/$ - see front matter © 2008 Elsevier Ltd. All rights reserved.
doi:10.1016/j.jfluidstructs.2008.03.004

As mentioned, work reported in Luo et al. (2007) was only for the case of a normal square cylinder. The objective of the present paper is to complement the above-mentioned work by looking into an aspect previously investigated by few (if any) researchers—the effects of angle of attack (α) on the transitional phenomena in the wake of a square cylinder. We feel that for a more complete understanding of the transition phenomena in the wake of a square cylinder, the nonzero α part is of equal importance. It will be interesting to find out, at an angle of attack at which the square cylinder does not exhibit top–bottom symmetry (i.e., at values of α that are neither 0° nor 45°), how the 2-D to 3-D transition in the wake will be affected.

2. Experimental methodology and set-up

As in Luo et al. (2007), three approaches were used to investigate the wake of an inclined square cylinder. They are hot-film anemometry for the identification of the critical Reynolds number and determination of flow characteristics; flow visualization for a general and visual understanding of the flow, including the symmetries and structures of different instability modes; and particle image velocimetry (PIV) for quantitative data which include the circulation and vorticity of primary and secondary vortices, etc.

In the present investigation, two flow facilities were used for different purposes. One is a vertical water tunnel and the other a horizontal water channel. Due to its ability to produce small changes in velocity, the vertical water tunnel was chosen for the investigation of the transition process in a cylinder wake via hot-film measurements. On the other hand, the flow visualization and PIV work were conducted in the horizontal water channel because of its highly transparent construction. Details of these two flow facilities as well as the various measurement techniques can be found in Luo et al. (2007) and Tong (2003).

3. Results and discussions

3.1. The boundaries of flow regimes at low Reynolds numbers

From a series of research work by Williamson and others on the circular cylinder wake transition, and by Luo and others on square cylinder wake transition, it is known that the wake transition process of a cylinder wake can be described well by the measurements of a single hot wire, and the division of different wake flow regimes can be described in reference to the two discontinuities in the Strouhal–Reynolds number relation. The first of the two discontinuities in the St–Re curve (at critical Reynolds number Re_{c1}) marks the inception of mode A instability, and the second (at critical Reynolds number Re_{c2}) the gradual transfer of energy from modes A to B instabilities. In addition, streamwise velocity fluctuations correspondingly exhibit distinct characteristics as Re increases through the wake transition regime.

In the current investigation on the wake of an inclined square cylinder, six angles of attack were investigated: $\alpha = 0^\circ$, 5°, 10°, 20°, 30° and 45°. The Reynolds number is defined as $Re = U_0 D/\nu$, where D is the projected width (across-flow dimension) of the cylinder. D is related to the side length D' of the cylinder via the relation $D/D' = \cos\alpha + \sin\alpha$. Accordingly, the Strouhal number is computed as $St = fD/U_0$. The cylinder aspect ratio (distance between the leading edges of the inward inclined end-plates over D) is approximately within the range of 38–50, depending on the actual angle of attack. The Reynolds number ranges from about 60 to 350.

The critical Reynolds numbers (Reynolds number at the onset of modes A and B instabilities) for the transition of a square cylinder wake were obtained through the determination of the St–Re relation. With the installation of the inclined end-plates mentioned, parallel vortex shedding was maintained during the 2-D wake regime, and the critical Reynolds numbers can be estimated accurately.

After the predominant vortex shedding frequency was determined at different Reynolds numbers, the St–Re relation is obtained and shown in Fig. 1. It can be seen that, even when the projected cross-flow dimension D was used as the length scale in computing both St and Re, the Strouhal number increases with the angle of attack when the Reynolds number is fixed at a certain value. However, the rate of increase reduces with the increase in angle of attack, and only a small difference exists between the curves for $\alpha = 30^\circ$ and 45°. At each fixed α, two discontinuities in the curve of St–Re, which mark the inception of mode A instability and the gradual transfer of energy from mode A to mode B instability, are observed. Compared with Re_{c1}, Re_{c2} is less well defined, as the transition process from mode A to mode B instability is relatively gradual. It is noted that the critical Reynolds number for the appearance of mode A instability (Re_{c1}) is approximately the same as the Reynolds number at which the Strouhal number begins to either slow down its increase

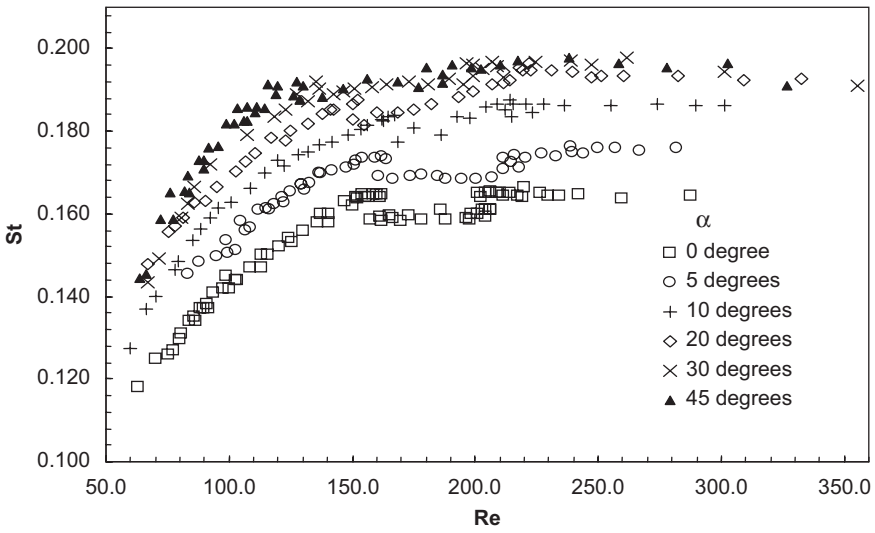

Fig. 1. The Strouhal–Reynolds number relationships for a square cylinder at different angles of attack.

Table 1
The critical Reynolds numbers at different angles of attack (α)

α (°)	Re_{c1}	Re_{c2}
0	160	204
5	165	215
6	166	≈200–220
10	167	217
20	154	214
30	136	200
45	127	190

Note:
1. The data shown above are the mean values of critical Reynolds numbers, with a variation of about 2 and 5 from the mean value for Re_{c1} and Re_{c2}, respectively.
2. For the case of $\alpha = 6°$, the Strouhal number was recorded only around the two discontinuities in the St–Re curve, from which Re_{c1} was identified accurately, while Re_{c2} was found to be around 200–220; no attempt was made to acquire a more accurate Re_{c2}.

(with Re) or approach some sort of asymptotic value. Since the Strouhal number is defined by $St = fD/U_0$ and in the present Strouhal number measurement experiment Re is increased by increasing U_0, it can be deduced that the increase in frequency outpaces that of free-stream velocity before the transition regime. The outpacing rate decreases with increasing Reynolds number and reaches zero (or may even become slightly negative in some cases) at around the inception of the secondary instability. The above results in the levelling off (or slight decrease) in St in the higher Re region of Fig. 1. The critical Reynolds numbers estimated for different α cases are tabulated in Table 1.

It can be seen that, when α increases, Re_{c1} increases from 160 (at $\alpha = 0°$) to 167 (at $\alpha = 10°$). Thereafter the trend reverses and Re_{c1} reaches a minimum of 127 at $\alpha = 45°$. Re_{c2} also displays a similar trend: it is about 204 at $\alpha = 0°$, increases to just below 220 at $\alpha = 10°$, and thereafter reduces gradually to 190 at $\alpha = 45°$. Sohankar et al. (1998) numerically studied the effects of angle of attack on the Reynolds number at the onset of vortex shedding (Re_c). Their data, together with the present Re_{c1} and Re_{c2} data, are plotted in a α-Re plot in Fig. 2. It can be seen that besides the low α range of less than 10°, where Re_c has practically the same magnitude at $\alpha = 0°$ and 10° (no data at intermediate α are available), a similar trend exists in all the three critical Reynolds numbers, although the variation in Re_c is somewhat smaller. Because of the relatively gentle variation in all three critical Re values with α, Fig. 2 enables one to approximately estimate the critical Reynolds numbers at an angle of attack where actual experimental data are not available.

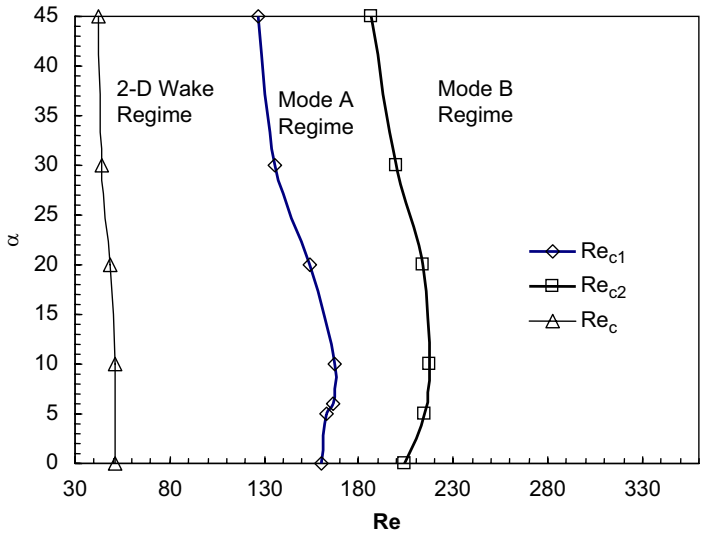

Fig. 2. Different flow regimes and critical Reynolds numbers for a square cylinder wake at different angle of attack. (*Note*: Re_c data are from Sohankar et al., 1998.)

When Reynolds numbers are increased from a fairly low value, the wake of a square cylinder exhibits characteristics of a 2-D wake (referred to as the "laminar vortex shedding regime" in Williamson (1996a)), modes A and B regimes in sequence until it finally becomes turbulent. It is not surprising to see that the velocity patterns that can be observed in the wake of a circular cylinder also exist in the wake of a square cylinder, including when it is at a nonzero angle of attack to the flow; although the ranges of Reynolds number involved are different. In the present paper, although altogether six angles of attack were investigated (0°, 5°, 10°, 20°, 30° and 45°), results for only three of them ($\alpha = 0°$, 10° and 45°) are presented. This is both for brevity and because of the similar main characteristics shared by all six sets of data. Despite the fact that results at $\alpha = 0°$ had already been discussed in details in Luo et al. (2007), they are still chosen as one of the three sets of results presented, because they serve as an important benchmark for reference/comparison; $\alpha = 10°$ and 45° were chosen as the other two angles of attack because from Fig. 2 it is seen that they represent the angle of attack at which the critical Reynolds numbers reach their maximum and minimum value, respectively. It was also noted that there is little justification in investigating the square cylinder wake at $\alpha > 45°$ because the flow will simply be the mirror image of that at $\alpha < 45°$ (for example, $\alpha = 40°$ and 50° are a mirror image pair).

Time traces of streamwise velocity of a square cylinder wake at different Reynolds numbers are shown in Fig. 3. At each angle of attack, three distinct velocity patterns were observed, corresponding to each of the three (2-D wake, modes A and B) flow regimes. In the 2-D wake regime (left column of Fig. 3), the variation of streamwise velocity with time is nearly perfectly periodic. In the mode A instability regime (centre column of Fig. 3), the regularity in the velocity fluctuation is generally present, but in some instances a sudden decrease in velocity magnitude (a glitch) is present. The presence of glitches is usually taken as an indication of the mode A flow regime. In the mode B instability regime (right column of Fig. 3), a more "uniform" disorder in the variation of velocity magnitude is present.

Velocity spectra in the wake of a square cylinder are shown in Fig. 4. Closely associated with the time traces, it can be seen that the spectra also display three kinds of patterns which correspond to 2-D wake, modes A and B regime. In the 2-D wake regime, a sharp peak is present in the spectrum, indicating that energy is concentrated within a rather narrow range around that the predominant frequency. In the mode A regime, a much broader "peak" is observed which suggests that energy was distributed over a wider frequency range. The spectra in the mode B regime are similar to those in the laminar regime, with a somewhat less sharp peak. According to Williamson (1996b), in circular cylinder wakes, if vortex dislocation is absent from the mode B flow regime, the transition from modes A to B is characterized by a twin-peak spectrum comprising of frequencies associated with modes A and B vortex shedding. It was already reported in Luo et al. (2007) that a similar situation appears in the transition of a square cylinder wake, and a twin-peak spectrum was observed for the case of square cylinder at $\alpha = 0°$ (at $Re = 198$). In the present paper, it is observed that similar twin-peak wake velocity spectra are also present in the nonzero angle of attack cases. However, it is interesting to note that the twin-peak spectra were observed at $Re = 198$, 216 and 177 for $\alpha = 0°$, 10° and 45°, respectively. At $Re = 198$ (there are no $Re = 198$ data in Fig. 4(b) and the closest Re is 192), at $\alpha = 0°$ the above-mentioned modes A to B transition twin-peak spectrum is observed. However, at $\alpha = 10°$ (Fig. 4(b)), the wake velocity spectrum looks more like

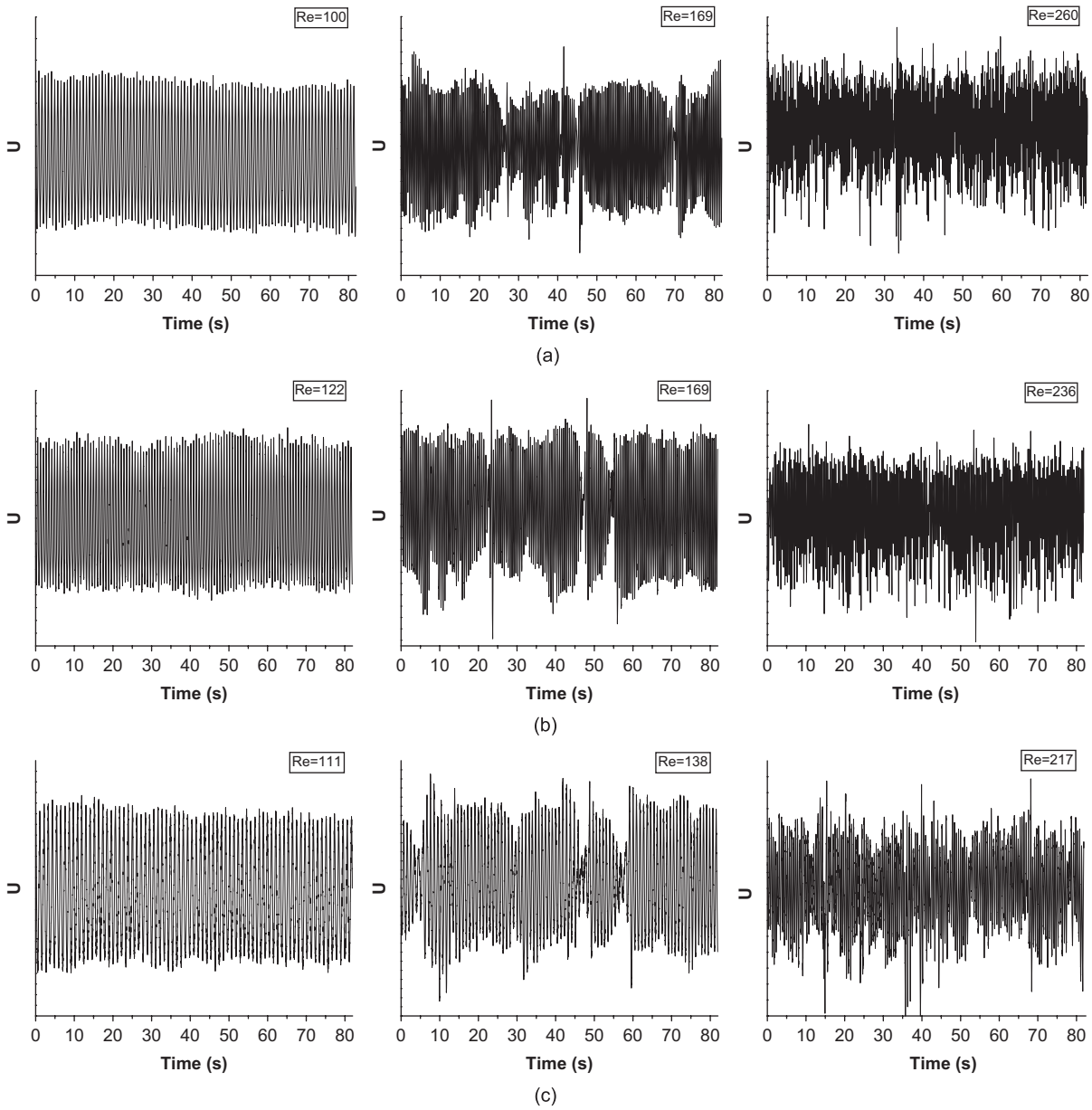

Fig. 3. The time traces of streamwise velocity in a square cylinder wake at different values of Re and α: (a) $\alpha = 0^\circ$, (b) $\alpha = 10^\circ$ and (c) $\alpha = 45^\circ$.

a typical (broad peak) mode A spectrum (the spectra at Re = 192 and 204 look fairly similar and are of the mode A broad peak type, so it is assumed that the same will apply to those at Re = 198). When α is increased to 45° (Fig. 4(c)), the spectrum at Re = 198 looks like a typical mode B spectrum, suggesting that the wake flow is already in the mode B regime. The above observation suggests that when the angle of attack of the square cylinder changes, although the essential characteristics of the transition wake remain, the sensitivity of the wake to various instability changes, resulting in changes in the boundaries of various flow regimes. This is consistent with the results shown in Fig. 2. In the literature, although there are a number of numerical studies that report on the wake transition phenomena of a square cylinder (DNS work of Sohankar et al. (1999), and the Floquet stability analysis work of Robichaux et al. (1999), Blackburn and Lopez (2003) and Blackburn et al. (2005)), to the authors' best of knowledge no similar work had been carried out on the wake of a square cylinder with its face at an angle of attack to the approach flow. When such studies become available, they will serve as interesting comparisons to the present experimental findings.

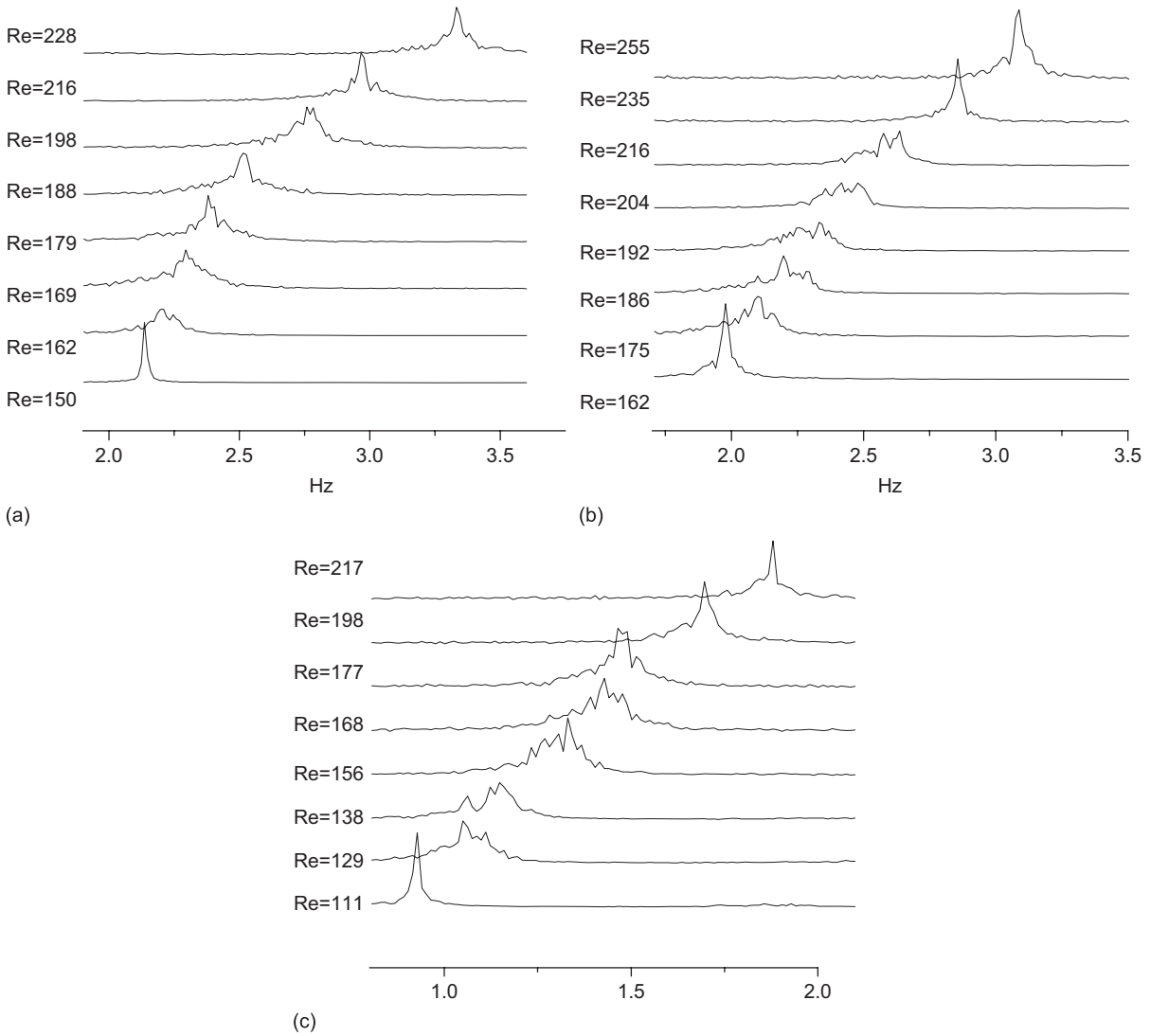

Fig. 4. The evolution of spectra from laminar to mode B regime at different α: (a) $\alpha = 0^\circ$, (b) $\alpha = 10^\circ$ and (c) $\alpha = 45^\circ$.

3.2. Flow visualization results

In the present investigation, the dye injection method was applied to visualize the wake structures of flow past a square cylinder. The square cylinder was terminated by end-plates inclined at an optimum angle (16–18° for the current set-up), and the three different flow regimes at the same three angles of attack ($\alpha = 0^\circ$, 10° and 45°) were investigated. It should also be pointed out that because there is only one slot (located on the top face) to release dye into the flow, only the top shear layer's primary vortices were observed.

In Fig. 5(a), the existence of three different flow regimes is clearly demonstrated for the case of $\alpha = 0^\circ$. A 2-D shedding pattern is observed for the case of $Re = 155$ and, as expected, there are no streamwise vortices between the primary vortices. When the Reynolds number was increased to 188, a typical mode A flow pattern can be observed. The primary vortex cores become wavy along the spanwise direction where some streamwise vortices were pulled out from the primary vortices. With the aid of a scale line, it can be seen that the wavelength of the streamwise vortices is around five times of the side length of the cylinder (D'). When the Reynolds number is increased to 244, which is known from hot-film measurements to fall within the mode B regime, much finer-scale streamwise vortices are seen. It is hard to determine the exact spanwise wavelength of the mode B streamwise vortices, but it should be around one to two times the side length of the cylinder.

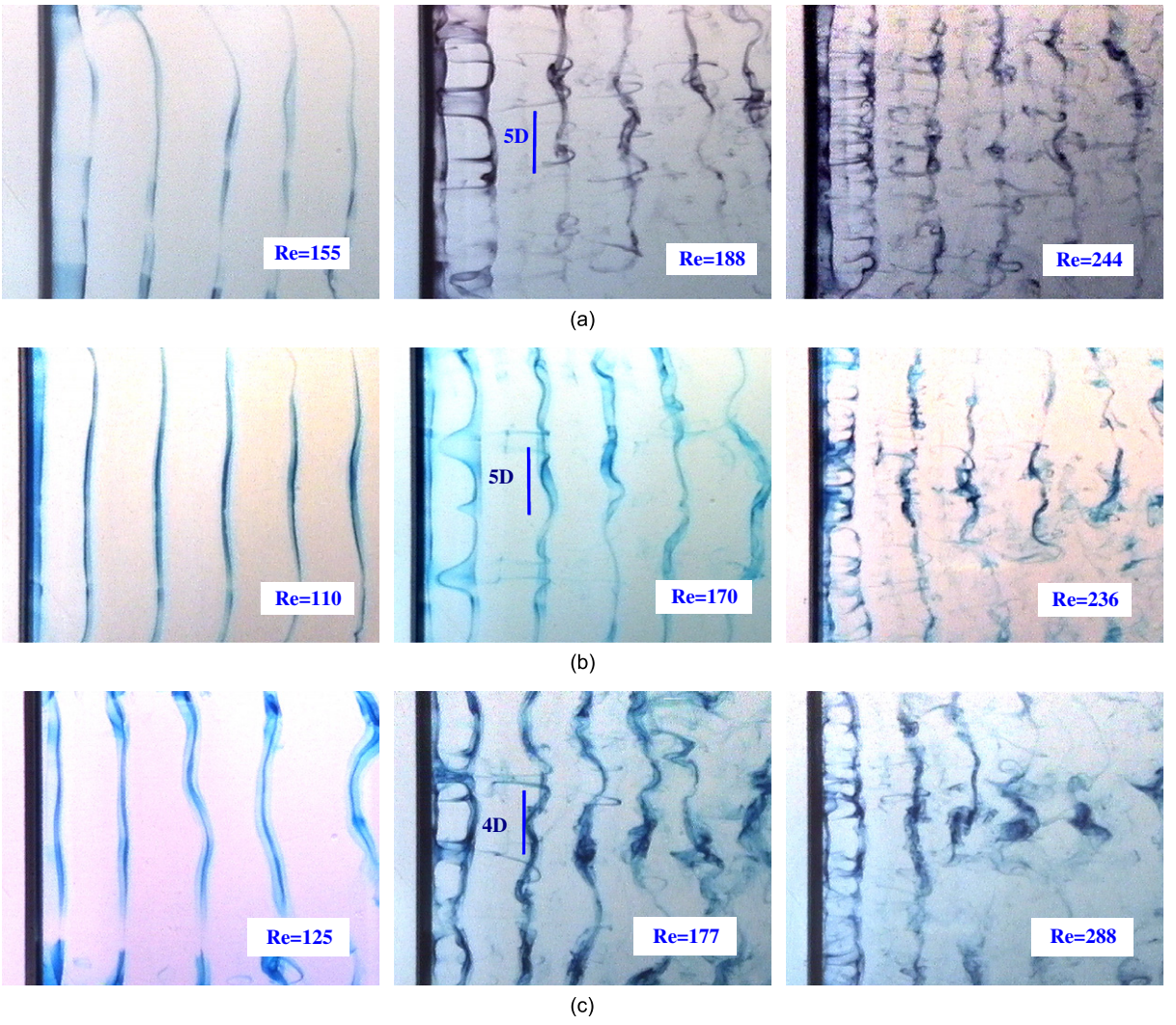

Fig. 5. The dye-visualized wake of a square cylinder wake at different values of Re and α. The flow is from left to right and the cylinder is near the left edge of the pictures α: (a) $\alpha = 0^\circ$, (b) $\alpha = 10^\circ$ and (c) $\alpha = 45^\circ$.

Not surprisingly, at other (nonzero) angles of attack, similar variations take place when the Reynolds number is increased. The distinct flow regimes for $\alpha = 10^\circ$ and 45° are shown in Fig. 5(b) and (c), respectively. For mode A instability, the spanwise wavelength is estimated to be around five and four times the projected width (D) of the inclined square cylinder for $\alpha = 10^\circ$ and 45°, respectively. Considering that $D/D' = 1$, 1.158 and 1.414 at $\alpha = 0^\circ$, 10° and 45°, respectively, it appears that the actual spanwise wavelength (in, say, mm) did not change significantly with α. For mode B instability, the spanwise wavelength is around 1–2D.

3.3. PIV measurements

In PIV measurements, the wake of the square cylinder was investigated at three Reynolds numbers and results are presented at the same three angles of attack as the above sections. For each case, three Reynolds numbers were chosen such that the first is in the mode A regime, and the other two are in the mode B regime (to distinguish, they are referred to as mode B_1 and mode B_2). Also similarly to previous sections, inclined end-plates (16–18°) were installed at the ends of cylinder to maintain parallel vortex shedding. Thus, end effects, if any, are assumed to be at a minimum.

The 3-D secondary vortices can be viewed as embedded within the primary vortices. They can therefore be observed both in the x–z plane and y–z plane. Due to the limitation of the current experimental set-up, only the y-component of

the secondary vortices (namely, ω_y) on the x–z ($y = 0$, the wake plane of symmetry) plane was measured and reported. In the above x, y, z are the (right-handed) orthogonal principal axes, with positive x in the free-stream direction, and z parallel to the cylinder axis.

In the current investigation, in order to achieve the required resolution level, four to six streamwise vortices along the cylinder span should be captured. Based on the spanwise wavelength of the streamwise vortices estimated from flow visualization, a spanwise length measuring about ten times and three times the projected width of the cylinder (D) is required in the modes A and B regime, respectively. The field of measurement is from $2D$ downstream of the cylinder, which is close to the downstream edge of the recirculation region.

Figs. 6 and 7 show the streamline patterns and vorticity contours of the secondary vortices at $\alpha = 10^\circ$ and 45°, respectively (results for $\alpha = 0^\circ$ can be found in Luo et al. (2007) and are not included here for brevity). In all of them, the velocity vectors were obtained in a frame of reference moving at 60% of the free-stream velocity (U_0). There are some common features in these figures. For example, in the streamline plots, the vortices in mode B regime (centre and right column) are usually clearly seen, while in the mode A regime (left column) the vortices are usually not obvious. The above suggests that the strain rate in the flow region near the secondary vortices is much higher in the mode B regime than in the mode A regime (quantitative data will be shown to support this point later in the section). In the vorticity plots, secondary vortices are arranged along a line that is parallel to the axis of the cylinder; and the sign of vortices alternates along the spanwise direction. On the other hand, vortices in the modes A and B regimes also exhibit differences. The most noticeable difference between modes A and B instability is the type of symmetry. In the vorticity plots, secondary vortices in the mode A regime are in a staggered arrangement along the x-direction, and the vortices change their sense of rotation over every half a shedding cycle (referred to as odd reflection-translation symmetry (or odd RT symmetry in short) in Robichaux et al. (1999)). On the other hand, streamwise vortices in the mode B regime have an in-line arrangement (the sense of rotation remains the same along the x-direction), and is referred to as even RT symmetry. In the cylinder spanwise direction, within each flow regime the distances between adjacent vortices appear to be fairly constant, but the distances involved are significantly different in modes A and B. For the case of a square cylinder at $\alpha = 0^\circ$, the above features of secondary vortices had been discussed, and detailed comparison made with the wake of a circular cylinder in Luo et al. (2007). They will not be repeated in the present paper. The interesting point to note here is that the results shown in Figs. 6 and 7 show that the above flow characteristics remain exactly the same at a nonzero angle of attack, although quantitative differences exist.

By using the autocorrelation method, the spanwise wavelength (λ_z) was estimated, each from about 40 sets of data. For mode A flow, λ_z was estimated to be around $5D$, while for mode B it is about $1D$. The final results for the square cylinder wake, together with results from different literature sources (including data for circular cylinders) are summarized in Table 2. The λ_z data shown in Table 2 are nondimensionalized by the cylinder diameter for the case of circular cylinder, and by the projected width D for the case of a square cylinder (at $\alpha = 0^\circ$ the projected width and the side length of the square cylinder are the same). For the present data, the spanwise wavelength for the case of $\alpha = 0^\circ$ is in good agreement with the results of Robichaux et al. (1999). In terms of variation with α, it is interesting to note that λ_z exhibits exactly a reverse trend in the modes A and B flow regimes. In the mode A flow regime, λ_z increases to a maximum at $\alpha = 10^\circ$ before decreasing towards $\alpha = 45^\circ$. In the mode B flow regime (both Re investigated), λ_z decreases to a minimum at $\alpha = 10^\circ$ before increasing toward $\alpha = 45^\circ$. At $\alpha = 45^\circ$ the difference between the modes A and B spanwise wavelengths becomes smaller.

In the present investigation, in all the α cases investigated, the spanwise wavelength in the mode B regime decreases with an increase in Reynolds number. This is consistent with the observation of Wu et al. (1994) for the circular cylinder wake.

In order to study the relations between the primary and secondary vortices, the peak value of vorticity (ω) and circulation (K) were measured. Unfortunately, due to the limitations in the present experimental set-up, only the z-component of the primary vortices and the y-component of the secondary vortices were measured. Some caution must be exercised when comparing them. Both vorticity and circulation were made dimensionless by D and U_0 in accordance to the following equations:

$$\zeta = \frac{\omega}{U_0/D}, \qquad \Gamma = \frac{K}{\pi D U_0}. \tag{1,2}$$

For each case, about 40 sets of data were averaged to obtain the representative value of peak-vorticity and its corresponding circulation. The final results are shown in Table 3.

The above data are also plotted in Fig. 8(a)–(c). For the circulation (Γ) data, it is not surprising to see that the circulation of the secondary vortices is significantly smaller than for their primary vortex counterparts, as the secondary vortices are supposed to originate from the primary ones. In the overall sense, both Γ_z and Γ_y decrease with Reynolds number. (There are fluctuations and there are "exceptions" to the above-mentioned decreasing trend.) For Γ_z, its

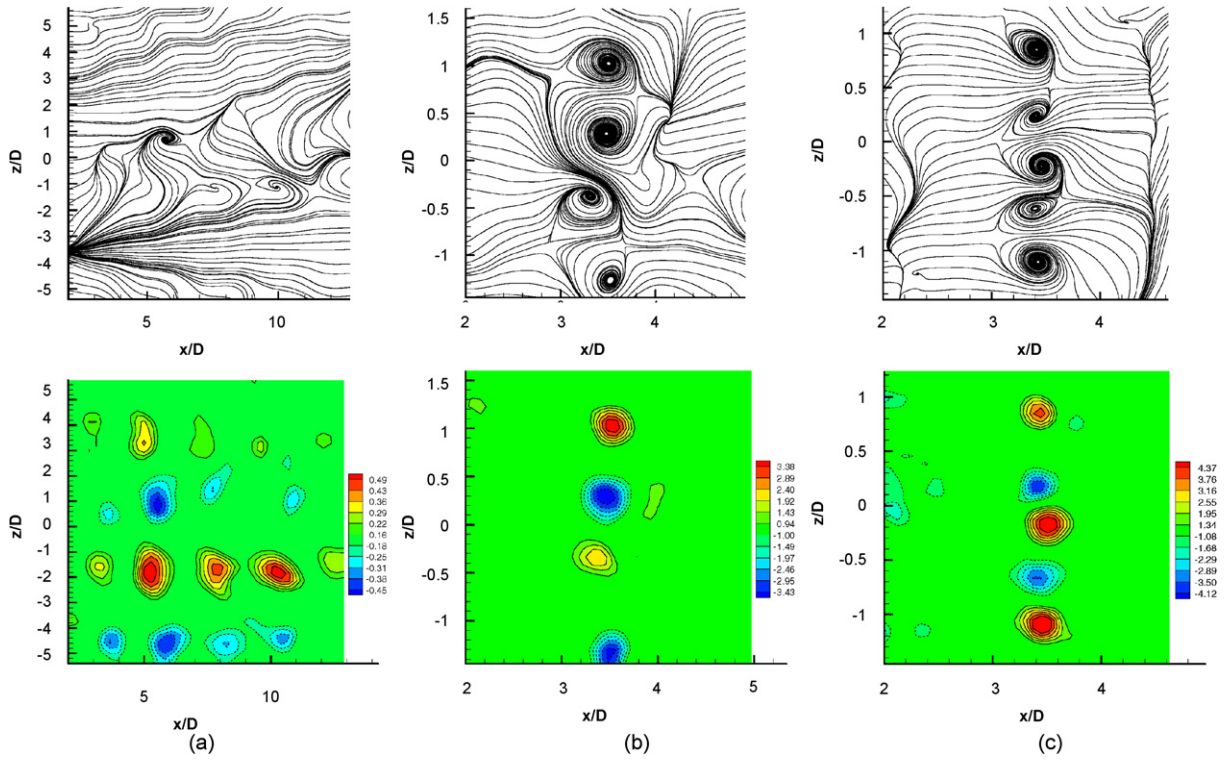

Fig. 6. Instantaneous streamline (top row) and vorticity contours (bottom row) of secondary vortices at $\alpha = 10^{\circ}$: (a) Re = 176, (b) Re = 269 and (c) Re = 436.

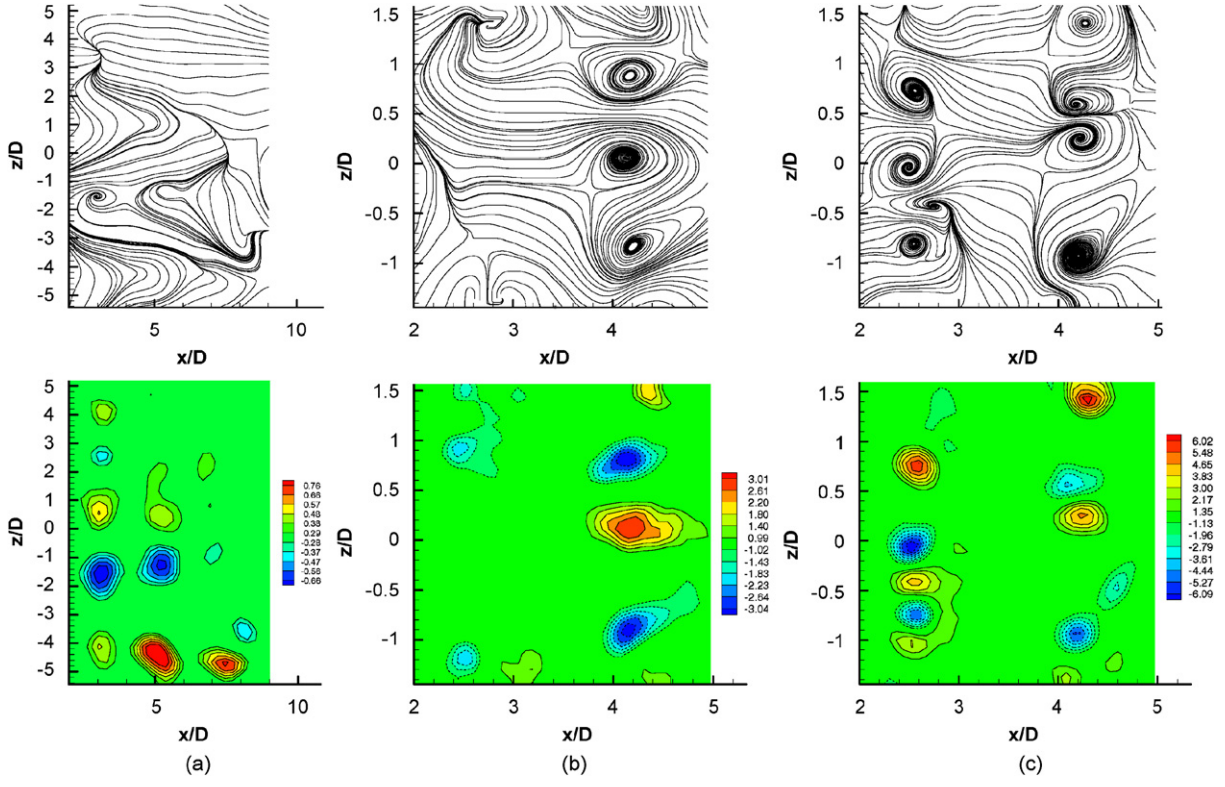

Fig. 7. Instantaneous streamline (top row) and vorticity contours (bottom row) of secondary vortices at $\alpha = 45^{\circ}$: (a) Re = 164, (b) Re = 227 and (c) Re = 396.

Table 2
Spanwise wavelength for circular cylinder and square cylinder

	Mode A	Mode B_1	Mode B_2
Literature			
Circular cylinder	3.96[a]	0.82[a]	
	4.5[b]	1[b]	
	4.01[d]	0.9–0.8[c] (decrease with increase in Re)	
Square cylinder $\alpha = 0^\circ$	5.22[e]	1.2[e]	
Current			
$\alpha = 0^\circ$	5.12	1.26	1.10
$\alpha = 10^\circ$	5.71	1.08	0.94
$\alpha = 45^\circ$	3.15	1.71	1.11

Note:
[a]Barkley and Henderson (1996), Floquet analysis.
[b]Brede et al. (1996), PIV.
[c]Wu et al. (1994), flow visualization.
[d]Williamson (1996b), flow visualization.
[e]Robichaux et al. (1999), Floquet analysis.

Table 3
The peak values of vorticity and circulation for primary and secondary vortices

Regime	Primary vortices			Secondary vortices		
	Re	ζ_z	Γ_z	Re	ζ_y	Γ_y
(a) $\alpha = 0^\circ$						
2-D wake	138	1.80 ± 0.05	1.05 ± 0.03			
Mode A	176	1.87 ± 0.07	1.17 ± 0.03	183	0.62 ± 0.03	0.28 ± 0.01
Mode B_1	231	2.39 ± 0.07	1.09 ± 0.02	228	2.68 ± 0.16	0.12 ± 0.01
Mode B_2	391	2.30 ± 0.13	0.94 ± 0.06	377	4.13 ± 0.16	0.17 ± 0.01
(b) $\alpha = 10^\circ$						
2-D wake	125	1.70 ± 0.08	0.99 ± 0.04			
Mode A	182	2.14 ± 0.14	0.94 ± 0.07	176	0.59 ± 0.02	0.36 ± 0.01
Mode B_1	265	2.39 ± 0.08	1.01 ± 0.02	269	3.51 ± 0.23	0.13 ± 0.01
Mode B_2	405	2.56 ± 0.13	0.83 ± 0.03	436	4.24 ± 0.20	0.11 ± 0.01
(c) $\alpha = 45^\circ$						
2-D wake	107	1.48 ± 0.05	1.04 ± 0.01			
Mode A	148	1.49 ± 0.06	0.93 ± 0.01	164	0.68 ± 0.07	0.29 ± 0.01
Mode B_1	230	1.82 ± 0.08	0.98 ± 0.02	227	3.22 ± 0.13	0.21 ± 0.02
Mode B_2	388	1.30 ± 0.08	0.75 ± 0.05	396	4.84 ± 0.23	0.17 ± 0.01

magnitude appears to reduce slightly with increasing α. This may be because the square cylinder becomes slightly more streamlined as α increases from 0° to 45°. For the vorticity data, in all three α cases investigated, ζ_z increases slightly with Re (one exception is the ζ_z data for modes B_1 and B_2 at $\alpha = 45^\circ$, which actually show a decrease with Reynolds number). On the other hand, ζ_y increases quite significantly with Re, with the magnitude in the mode B regime much larger than the one in the mode A regime. As a result, in all three α cases investigated, $\zeta_y < \zeta_z$ in the mode A regime, but $\zeta_y > \zeta_z$ in the mode B regime. This is consistent with the "increase in straining of the secondary vortices in the mode B regime" mentioned earlier in this paper. In terms of effects of α, ζ_z appears to reduce slightly with α (following Γ_z), whereas ζ_y appears to increase slightly with α, suggesting that, when α increases while the magnitude of circulation shed is slightly reduced, the "strain effect" of the secondary vortices slightly increases.

Overall, despite some quantitative differences in the various data, the main flow features appear to remain unchanged when α increases from 0° to 45°.

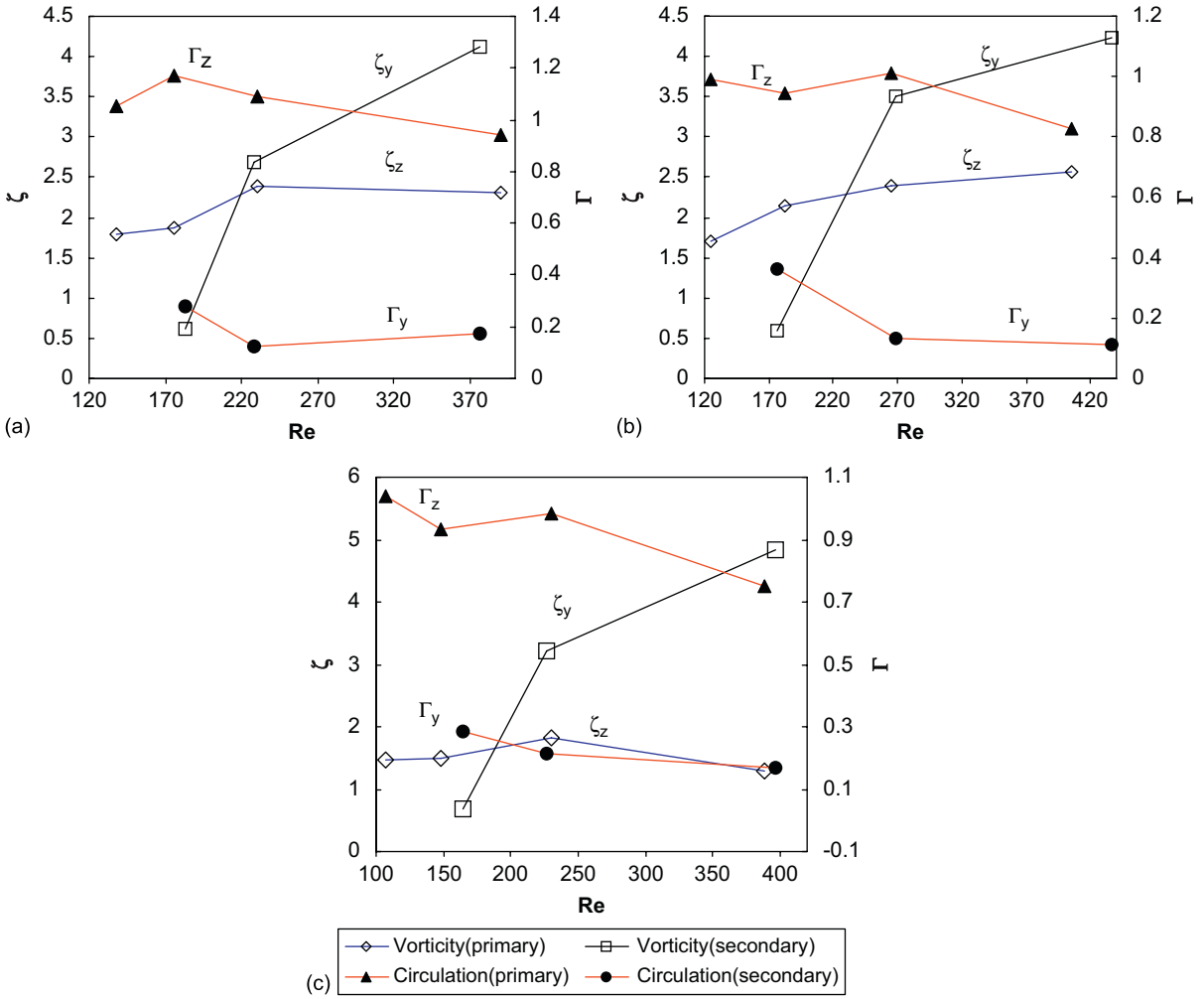

Fig. 8. The comparison of vorticity and circulation between primary vortices and longitudinal vortices at various angles of attack: (a) $\alpha = 0^\circ$, (b) $\alpha = 10^\circ$ and (c) $\alpha = 45^\circ$.

4. Conclusions

In the Re range investigated (approximately 60–350), St increases with Re, with the rate of increase decreasing as Re increases. The same trend was also observed when the square cylinder was inclined to the free stream. The above trend is consistent with the ($\alpha = 0^\circ$) results reported in the literature. At a certain fixed Re, St increases with α, in agreement with the general trend that streamlined bodies shed vortices faster than bluff bodies.

The two discontinuities in the St–Re curve which mark the onset of modes A and B instabilities are present at all the α investigated. Both Re_{c1} and Re_{c2} vary with α, in a way that both reach their respective maximum at α near 10°. More details were shown in Table 1. The α-Re plot in Fig. 2 enables one to have a quick estimate of the critical Reynolds number when actual experimental data are not available. As a previous (low Re) work (Luo et al., 2003) suggests that one of the separated shear layers reattaches at $\alpha \approx 6^\circ$, it is thought that the maxima in Re_{c1} and Re_{c2} may be related to flow reattachment, but further investigation is necessary.

Wake velocity-time traces exhibit the three unique patterns in the 2-D wake, modes A and B regimes. The above also apply to cases involving inclined square cylinders.

By using dye to visualize the cylinder wake in the x–z plane, the spanwise wavelength λ_z was estimated to be $5D'$, $5D$ and $4D$ at $\alpha = 0^\circ$, 10° and 45°, respectively, in the mode A regime. In the mode B regime, the spanwise wavelength was estimated to be 1–$2D'$ and 1–$2D$ for the normal and inclined square cylinders, respectively. PIV (quantitative) data are

in fairly good agreement with flow visualization. PIV data reveal that, when α increases from 0° (the mode A regime), λ_z increases to a maximum at $\alpha = 10^\circ$, before it decreases with further increases in α. In contrast, in the mode B regime, λ_z decreases to a minimum at $\alpha = 10^\circ$, before it increases with further increase in α. Compared to a normal square cylinder, the difference between the actual spanwise wavelength between the modes A and B regimes has become smaller at $\alpha = 45^\circ$. For all the α investigated, the mode B λ_z decreases with Re.

Generally speaking, the Re dependence of both the primary and secondary vortices shows a similar trend at all the α investigated. In all the cases, the magnitudes of Γ_y are smaller than their corresponding Γ_z, which is expected. Both Γ_z and Γ_y decrease with Re. While ζ_z increases slightly with Re, ζ_y increases significantly with Re. On the issue of α dependency, Γ_z reduces slightly with α. While ζ_z reduces slightly with α, ζ_y shows a slight increase with α. At all the angles investigated, $\zeta_y < \zeta_z$ in the mode A regime, but the trend is reversed and $\zeta_y > \zeta_z$ in the mode B regime.

Acknowledgement

Author X.H. Tong was a recipient of the National University of Singapore Research Scholarship. The award of this scholarship is gratefully acknowledged.

References

Barkley, D., Henderson, R.D., 1996. Three-dimensional Floquet stability analysis of the wake of circular cylinder. Journal of Fluid Mechanics 322, 215–241.

Blackburn, H.M., Lopez, J.M., 2003. On three-dimensional quasiperiodic Floquet instabilities of two-dimensional bluff body wakes. Physics of Fluids 15 (8), L57–L60.

Blackburn, H.M., Marques, F., Lopez, J.M., 2005. Symmetry breaking of two-dimensional time-periodic wakes. Journal of Fluid Mechanics 522, 395–411.

Brede, M., Eckelmann, H., Rockwell, D., 1996. On secondary vortices in the cylinder wake. Physics of Fluids A 8 (8), 2117–2124.

Luo, S.C., Chew, Y.T., Ng, Y.T., 2003. Hysteresis phenomenon in the galloping osciallation of a square cylinder. Journal of Fluids and Structures 18, 103–118.

Luo, S.C., Tong, X.H., Khoo, B.C., 2007. Transition phenomena in the wake of a square cylinder. Journal of Fluids and Structures 23, 227–248.

Robichaux, J., Balachandar, S., Vanka, S.P., 1999. Three-dimensional Foquet instability of the wake of square cylinder. Physics of Fluids 11, 560–578.

Sohankar, A., Norberg, C., Davidson, L., 1998. Low-Reynolds number flow around a square cylinder at incidence: study of blockage, onset of vortex shedding, and open boundary conditions. International Journal for Numerical Methods in Fluids 26, 39–56.

Sohankar, A., Norberg, C., Davidson, L., 1999. Simulation of three-dimensional flow around a square cylinder at moderate Reynolds numbers. Physics of Fluids 11 (2), 288–306.

Tong, X.H., 2003. Transition phenomena in the wakes of cylinders. Ph.D. Dissertation, National University of Singapore.

Williamson, C.H.K., 1996a. Vortex dynamics in the cylinder wake. Annual Review of Fluid Mechanics 28, 477–539.

Williamson, C.H.K., 1996b. Three-dimensional wake transition behind a cylinder. Journal of Fluid Mechanics 328, 345–407.

Wu, J., Sheridan, J., Soria, J., Welsh, M.C., 1994. An experimental investigation of streamwise vortices in the wake of a bluff body. Journal of Fluids and Structures 8, 621–635.